Tissue and Cell 93 (2025) 102631

Contents lists available at ScienceDirect

Tissue and Cell

journal homepage: www.elsevier.com/locate/tice

Detection of the nuclear translocation of androgen receptor using quantitative and automatic cell imaging analysis

Lanlan Bai [a], Tao Wu [a], Mizuki Fukasawa [b], Sayo Kashiwagi [c], Haruka Tate [a], Taku Ozaki [a], Eriko Sugano [a], Hiroshi Tomita [a], Tsuyoshi Ishii [c,*], Takuya Akashi [b,*], Tomokazu Fukuda [a,*]

[a] Graduate School of Science and Engineering, Iwate University, 4-3-5 Ueda, Morioka, Iwate 020-8551, Japan
[b] Neuro-AI Integration Science Laboratory, Faculty of Environmental, Life, Natural Science and Technology, Okayama University, 3-1-1, Tsushima-naka, Kita-ku, Okayama 700-8530, Japan
[c] Rohto Pharmaceutical Co., Ltd., Basic Research Development Division, 6-5-4 Kunimidai, Kizugawa, Kyoto 619–0216, Japan

ARTICLE INFO

Keywords:
Dermal papilla cell
Nuclear translocation
Androgen receptor
Live cell imaging
Digital image analysis
Quantitation algorithm

ABSTRACT

Testosterone signaling mediates diseases such as androgenetic alopecia and prostate cancer and is controlled by the activation of the androgen receptor (AR) and nuclear translocation of the ligand-receptor complex. This study established an immortalized dermal papilla cell line that stably expresses the AR labeled with a monomeric green fluorescence marker. The cells expressed the histone H2B protein as visualized using a red fluorescence marker, enabling the Detection of nuclear translocation under live cell conditions using image analysis. The AR was observed to be translocated from the cytoplasm to the nucleus of cells after stimulation with dihydrotestosterone (DHT). The signal intensity of the nuclear/cytoplasm ratio was analyzed using automatic image analysis and a newly developed algorithm. The quantitation method to detect nuclear translocation revealed that the AR nuclear signal plateaued approximately 20 min after DHT exposure. Our developed method has the potential to save human labor by the automatic process of the image.

1. Introduction

Nuclear receptors play a critical role in ligand-dependent transcriptional regulation. The androgen receptor (AR) is a nuclear receptor associated with various diseases, including prostate cancer (Fizazi et al., 2014) and androgenic alopecia (AGA) (York et al., 2020). Testosterone and dihydrotestosterone (DHT) are natural ligands of the AR, with the affinity of DHT to AR being stronger than that of testosterone. DHT production is regulated by the enzymatic activity of 5-alpha reductase (Said and Mehta, 2018). Inhibiting the activity of 5-alpha reductase results in the loss of DHT, which is effective at inhibiting the progression of AGA. Inhibitors of 5-alpha reductase, such as finasteride and dutasteride, have been developed to treat AR-dependent diseases (Choi et al., 2016).

After dimerization of the AR and complex formation with a ligand in the cytoplasm, the AR is translocated to the nucleus of cells (Nadal et al., 2017). Gorge at al showed that the androgen receptor fused with the GFP fluorescence tag showed the nuclear translocation in COS7 cells after the ligand stimulation (Georget et al., 1997). Stenoin et al. showed the function of Polyglutamine-Expanded Androgen Receptors Form using Hela cell (Georget et al., 1997). Tyagi et al. showed that GFP-fused androgen receptors showed ligand-dependent translocation using PC3, Hela, and COS1 cells (Tyagi et al., 2000). Tomura et al. showed the subnuclear three-dimensional image analysis of the Androgen Receptor which fused to green fluorescence protein (Tomura et al., 2001). Saito et al. also showed the detailed cellular localization of DHT bound AR-GFP molecules in COS7 cells using a three-dimensional imaging technique (Saitoh et al., 2002). Marcelli et al. and Szafran et al. showed that automatic High throughput microscopy can be applied to cell imaging and translocation of AR under the transient expression in Hela cell (Marcelli et al., 2006; Szafran et al., 2008). However, most of the listed studies detect the transient expression after the transfection of plasmids into Hela or COS7 cells. Although the transfection efficiency of plasmids into COS7 or Hela cells is relatively high, the efficiency of lipofection into primary cells is markedly lower. To solve this problem, Chiu *et al.* determined the kinetics of the nuclear translocation of AR in PC3 and LNCaP prostate cancer cell lines under stable conditions using multimodal image correlation spectroscopy (mIS) (Chiu et al., 2016).

* Corresponding authors.
E-mail addresses: ishii@rohto.co.jp (T. Ishii), akashi@okayama-u.ac.jp (T. Akashi), tomof009@iwate-u.ac.jp (T. Fukuda).

https://doi.org/10.1016/j.tice.2024.102631
Received 7 August 2024; Received in revised form 30 October 2024; Accepted 18 November 2024
Available online 10 December 2024

However, mIS requires the setting up of special devices. The chromosome conditions of cancer-derived cell lines, such as LNCaP, caused frequent chromosome instability due to loss of function in the p53 gene, consistent with the critical role of p53 as a tumor suppressor (Deppert, 2007). In contrast to cancer cell lines, the expression of the R24C mutant, cyclin-dependent kinase 4 (CDK4), cyclin D1, and telomerase reverse transcriptase (TERT) (hereafter referred to as K4DT cells from the top characteristics of genes) enabled the establishment of an immortalized dermal papilla cells (DPCs) with minimal chromosome abnormality (Fukuda et al., 2020) and a small alteration of gene expression compared with the immortalization with the SV40T or E6E7 human papillomavirus oncoproteins (Fukuda et al., 2021). Owing to these observations, we hypothesized that the establishment of cells that stably express AR with a fluorescence tag in immortalized DPC with K4DT might help elucidate the kinetics of the nuclear translocation of AR, thereby enabling the screening of candidate inhibitors of nuclear translocation via a high-throughput study.

In our previous study, the expression level of endogenous AR was found to be very low, even after two passages of commercially obtained parental DPCs (Fukuda et al., 2020). Consistent with our finding, the endogenous expression level of AR in rat derived DPCs is reported to be markedly lower at passage 4 (Kwack et al., 2008). Although the detailed mechanism is unclear, the expression level of AR is substantially downregulated due to the cell passage procedure for primary DPCs. We also confirmed that the immortalized DPCs are negative for endogenous AR using real time PCR (Fukuda et al., 2020). To compensate for AR expression, we introduced AR with a hemagglutinin (HA) tag through retrovirus gene transfer into immortalized DPCs. One of the major downstream genes of AR signaling, *DKK1*, was found to be highly upregulated after the exogenous introduction of HA-tagged AR, suggesting that the downstream pathway of AR is intact even after silencing of endogenous AR (Fukuda et al., 2020). Establishing cell lines that stably express AR with fluorescence tags would be a valuable tool to find out the low molecular inhibitor of the AR signaling pathway.

2. Material and methods

2.1. Cell culture

As previously reported, we used immortalized human follicle DPCs expressing mutant CDK4, cyclin D1, and TERT (Fukuda et al., 2020). We commercially obtained primary DPCs from PromoCell (Heidelberg, Germany) through Takara Bio (Shiga, Japan). In the immortalized DPCs, we previously found that the expression of endogenous AR is almost undetectable via real time PCR. Detailed information regarding immortalized DPCs can be found in our previous report (Fukuda et al., 2020). DPCs were cultured in a follicle DPC medium (cat. no. C-26500, PromoCell,) with a supplement pack (cat. no. C-39620, PromoCell). DPCs were seeded in a six-well plate with 2 mL of medium per well. The cells were cultured at 37 ℃ in a humidified atmosphere containing 5 % CO_2.

2.2. Preparation of the recombinant viruses and genetic introduction

We used recombinant retroviruses expressing mStrawberry-H2B and Azami green-Human AR to detect cellular localization of the nuclei and AR. The retroviruses were packaged via the transient expression of pQCXIN-mStrawberry-H2B (Takara-Bio, Shiga, Japan) and pQCXIP-Azami-AR (Takara-Bio) in 293 T cells and pCAG-VSVG-Rsv-Rev and pCL-gag-pol were used as the packaging plasmids (Donai et al., 2013). The recombinant viruses were exposed to the immortalized DPCs for 48 h. Single-cell cloning was used to select the target cells. Cells were seeded in 10-mm dishes at 100 cells per dish. The brightest fluorescent cell colonies were selected using cloning rings.

2.3. Genomic PCR

Genomic DNA was extracted from cells using the NucleoSpin Tissue Kit (cat. no. 740952, Takara Bio). PCR was performed with 100 ng of template DNA, 1X KOD-FX neo PCR buffer (KFX- 201; Toyobo, Osaka, Japan), 0.4 μM dNTPs (KFX-201, Toyobo), 0.5 U KOD-FX neo (KFX-201, Toyobo), and 0.3 μM of each primer, according to the manufacturer's protocol. The following primers were employed: mStrawberry-H2B forward 5'-TCCCACAACGAGGATTACACCA-3' and reverse 5'-CCGGATCCTCAGCTAGTCA-3'; Azami-AR forward 5'-GAACGGCCA-CAACTTCGTGA-3' and reverse 5'-CCTTCAGCACGCCATCCTC-3'; and TSC2 forward 5'- AAACCGAGCCCCATTTGACC-3' and reverse 5'-TGGTCGTAGCGGAATCGAGGAT-3'.

2.4. RT-PCR

Total RNA was extracted from wild type DPCs, immortalized DPC (K4DT), immortalized DPC with H2B, immortalized DPC with H2B and Az AR clone7, immortalized DPC with H2B and Az AR clone10 using a NucleoSpin RNA kit (Takara Bio) according to the manufacturer's protocol. RNA samples were reverse transcribed into cDNA using a High Capacity RNA-to-cDNA Kit (Thermo Fisher Scientific) according to the manufacturer's instructions. Briefly, 2 μg of RNA samples were mixed with an RT reaction mixture containing the enzyme to incubate the reaction at 37°C for 60 min and 95°C for 5 min to obtain cDNA. PCR was performed with 100 ng of template DNA, 1X KOD-FX neo PCR buffer (KFX- 201; Toyobo, Osaka, Japan), 0.4 μM dNTPs (KFX-201, Toyobo), 0.5 U KOD-FX neo (KFX-201, Toyobo), and 0.3 μM of each primer, according to the manufacturer's protocol. We used the same primers for the Detection from RT-PCR with genomic PCR, Azami-AR, and mStrawberry-H2B. For the Detection of GAPDH(glyceraldehyde-3-phosphate dehydrogenase) internal control, we used the GAPDH forward: 5′-CCAGAACATCATCCCTGCCT-3′, and reverse: 5′-TCAAAGGTG-GAGGAGTGGGT-3′. As the negative control, we also set up the samples without reverse transcriptase, such as reverse transcription minus.

2.5. Western blotting

Western blotting was performed to detect the expression of proteins encoded by Azami-AR and mStrawberry-H2B. The cells were lysed in HIPS buffer, which comprised 50 mM Tris-HCl (pH 7.4), 0.15 M NaCl, 1 % Triton X-100, 2.5 mg/mL sodium deoxycholate, and protease inhibitor (Fukuda et al., 2005, 2000). Mouse anti-α-tubulin (1:1000, no. sc-32293, Santa Cruz Biotechnology, Dallas, TX, USA), mouse anti-AR (1:2000, no. sc-7305, Santa Cruz Biotechnology, Dallas, TX, USA), anti-monomeric Azami-Green 1 pAb (1:1000, no PM052M, Medical & Biological Laboratories Co. Ltd., Nagoya, Aichi, Japan), and anti-RFP mAb (1:1000, no M204–3, Medical & Biological Laboratories Co. Ltd., Nagoya, Aichi, Japan) were used as the primary antibodies. A goat fab anti-mouse IgG-linked horseradish peroxidase (1:2000, code no. 330, Medical & Biological Laboratories Co. Ltd., Nagoya, Aichi, Japan) or a goat fab anti-rabbit IgG-linked horseradish peroxidase (1:2000, code no. 458, Medical & Biological Laboratories Co. Ltd.) was used as the secondary antibody. Pierce ECL (Thermo Fisher Scientific, Waltham, MA, USA) was used to visualize the signals, and an Image Quant LAS-4000 Mini system (GE Healthcare, Chicago, IL, USA) was used to visualize the images.

2.6. DHT treatment

The follicle DPC medium (cat. no. C-26500, PromoCell) was replaced with DMEM/Ham's F-12 phenol red and serum-free medium (code 11582–05, Nacalai Tesque) approximately 24 h before DHT treatment. DHT (Stanolone, code A0462, Tokyo Chemical Industry, Tokyo, Japan) was diluted to 10 μM with dimethyl sulfoxide and PBS and DHT 1/100 of DMEM/Ham's F-12 phenol red and serum-free medium to achieve a

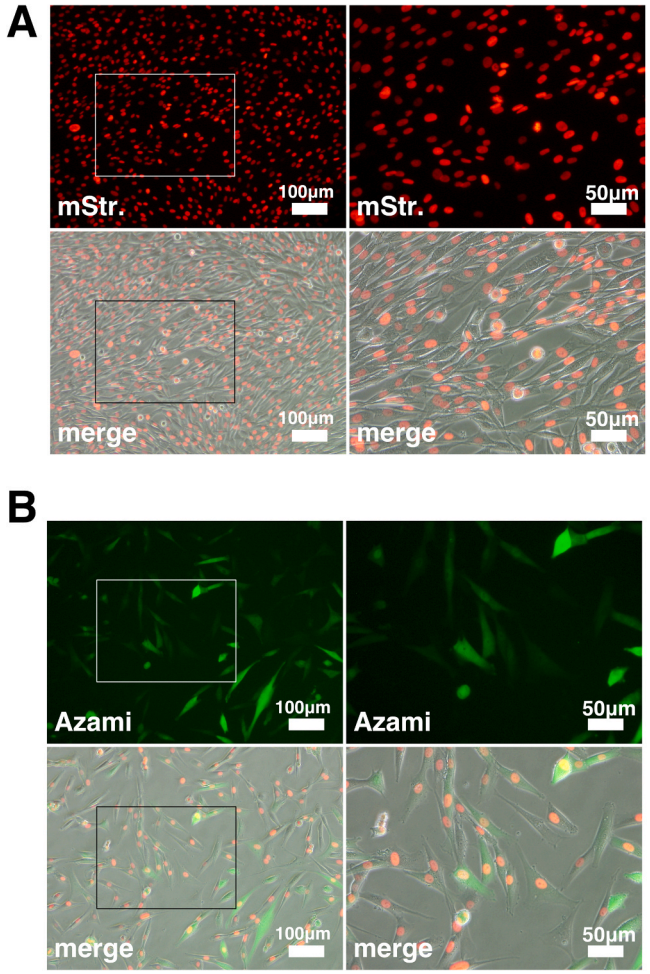

Fig. 1. Introduction of mStrawberry-labeled histone H2B protein and Azami green-labeled androgen receptor (AR) via retrovirus gene transfer into immortalized DPCs. A, Detection of mStrawberry-labeled histone H2B protein under a fluorescence microscope in immortalized human dermal papilla cells (HFDPCs). B, Detection of Azami green-labeled AR; the expression level of AR varies among multiple cells in the mass cell population resistant to G418 and puromycin.

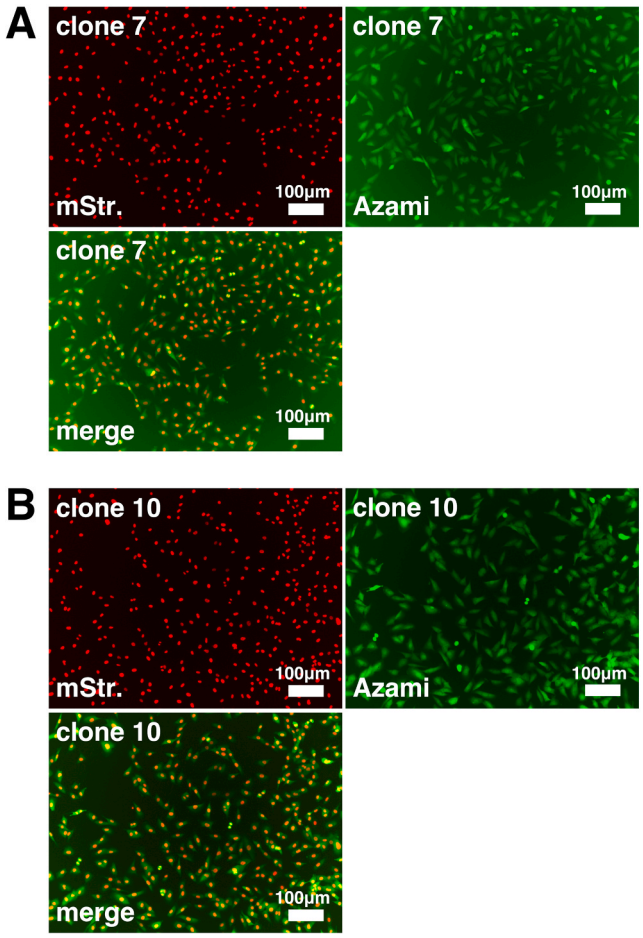

Fig. 2. Cloned human dermal papilla cells (HFDPCs) stably express both mStrawberry-labeled H2B and Azami green-labeled androgen receptor. A, Fluorescence imaging of clone 7. Red, green, and merged image with DIC (Differential Interference contras). B, Fluorescence imaging of clone 10. Red channel, green channel, and merged image with DIC.

concentration of 100 nM. Treatment with DHT was performed for 8 hours. We also treated cells with 5 nM DHT. The time-lapse analysis was performed for up to 4 hours after exposure to DHT. In addition to the DHT, we also finished the treatment with testosterone. The cells were treated with 100 nM of testosterone.

2.7. Time-lapse imaging

We used a fluorescence microscope (BZ-8100, KEYENCE, Osaka, Japan) to detect the translocation of AR using time-lapse videos. An incubation system was employed for microscopy (TOKAI HIT, Shizuoka, Japan) to confirm that the cell culture conditions were maintained at 37 ℃ in a humidified atmosphere with 5 % CO_2. To reduce the influence of fluorescence fading, the MF10 and MF20 filters were used, and antifade (P36975, Thermo Fisher Scientific) was added to the medium to reduce the fade of mStrawberry and Azami green. Images were captured every 40 s, and time-lapse videos were made at 15 fps (Olympus, Tokyo, Japan).

2.8. Signal quantitation in the nuclei and cytoplasm

This quantitation method comprised three steps: nuclei detection, nuclei tracing, and signal intensity detection in the nuclei and cytoplasm. To detect the nuclei, images obtained from the red channel were processed. The original frame of the red channel was processed into a binarization process after grayscale conversion. The threshold for binarization was obtained from the optimized value, which enabled the clearest edge of the nuclei. The unique ID number was placed against the cells from the binarized images. The nuclei were traced with location information on the image. By comparing the first frame with the subsequent frames, we determined the trace direction of the cell. We selected the cells with the ID number, which successfully allowed tracing from the first to the last frame. After obtaining the location information of the nuclei from the red channel, we detected the fluorescence intensity in the nuclei in the green channel. We then expanded the nuclei mask to approximately 5 pixels. We also measured the fluorescence intensity of the expanded area and scored it as the signal intensity of the cytoplasm. The nuclear/cytoplasmic fluorescence intensity ratio was obtained from 20–30 cells, enabling the transition throughout the time-lapse analysis.

3. Results

3.1. Establishment of immortalized dermal papilla cells using two colored fluorescence

As previously reported, the expression of the AR gene was

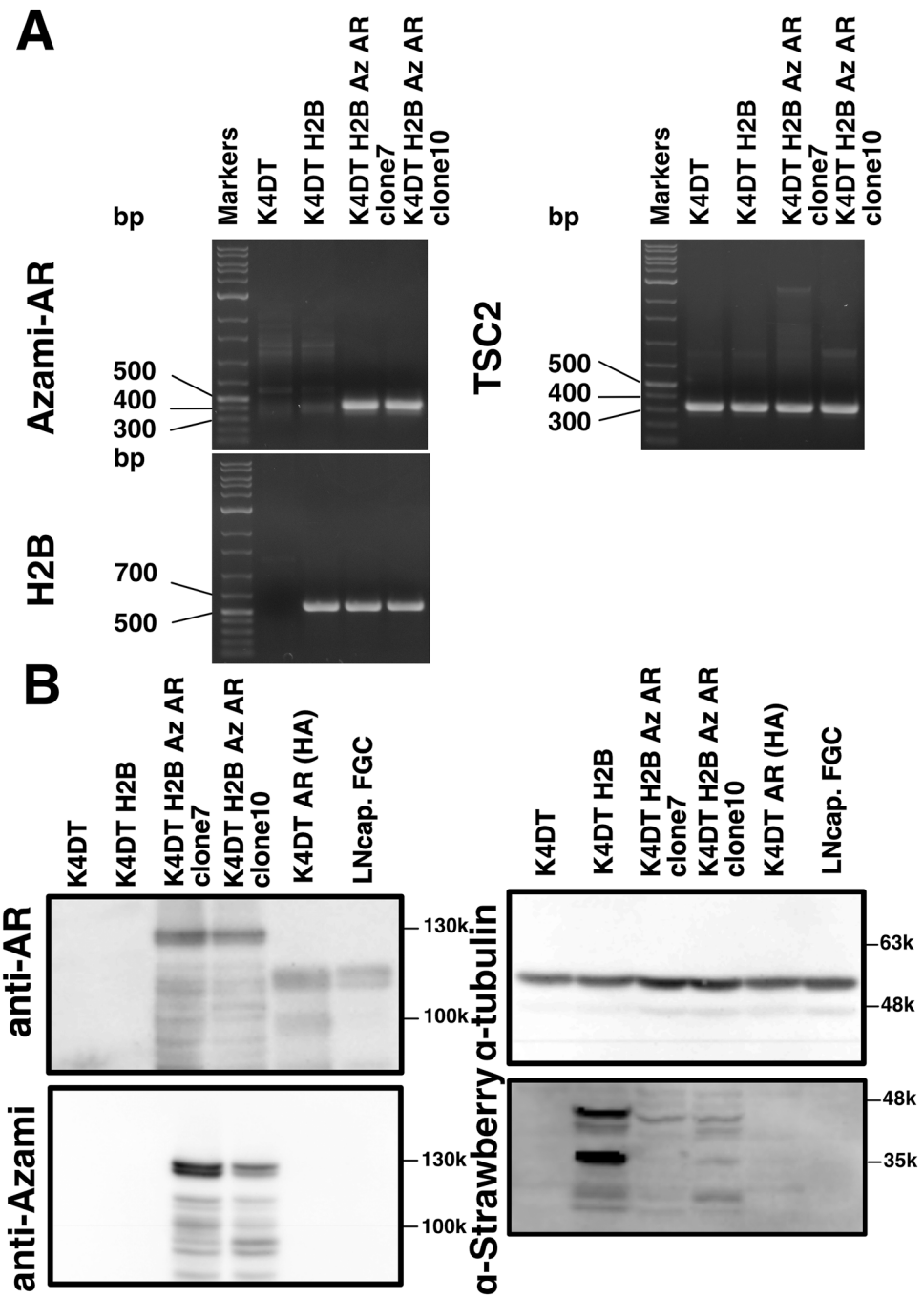

Fig. 3. Detection of the expression cassettes of mStrawberry-labeled H2B and Azami green-labeled androgen receptor in HFDPCs via PCR and western blotting. A, PCR amplification of the genomic DNA of parent immortalized DPCs (K4DT) and immortalized DPCs expressing mStrawberry-labeled H2B (K4DT H2B) and the cloned immortalized DPCs expressing mStrawberry-labeled H2B and Azami green-labeled AR (K4DT H2B Az AR clone 7, 10). B, Detection of Azami green-labeled androgen receptor in HFDPCs at the protein level. Left panels, Detection of parent K4DT expressing mStrawberry-labeled H2B, cloned immortalized DPCs expressing mStrawberry-labeled H2B and Azami green-labeled AR (K4DT H2B Az AR clone 7, 10), immortalized DPCs expressing the HA protein-tagged androgen receptor (positive control) detected using the AR antibody. Protein detection using the anti-Azami antibody. Right panel, alpha-tubulin western blot and mStrawberry western blot.

undetectable in primary and immortalized DPCs using real time PCR (Fukuda et al., 2020). To compensate for the silenced AR, we inserted an AR with an Azami green monomer fluorescence tag into the QCXIP retrovirus vector (Fig. S1A). We also inserted histone H2B into the QCXIN retrovirus vector with a mStrawberry fluorescence tag (Fig. S1A). We chemically synthesized the insert cDNA of AR with the Azami green monomer and histone H2B with mStrawberry. Interestingly, AR and histone H2B with the fluorescence tags were expressed in the bacteria and pUC57 shuttle vector, and green and red fluorescence tagged proteins were detected even in the bacterial colonies (Fig. S1B, C, and D). The fluorescence protein tag sometimes forms a dimer, resulting in a false positive signal in imaging analysis (Zacharias et al., 2002). Zacharias et al. revealed that introducing a mutation at aa 206 in GFP prevents this artifact, enabling the maintenance of the monomer form (Zacharias et al., 2002). To avoid the dimerization of the fluorescence tag, we selected monomer-type Azami green and mStrawberry.

After packaging the retroviruses, the recombinant retrovirus was introduced into immortalized DPC cells expressing mutant CDK4, Cyclin

D1, and TERT (DPCs-K4DT). As expected, although parent DPCs-K4DT did not exhibit any fluorescence (Fig. S2), DPCs-K4DT cells expressing histone H2B with mStrawberry displayed an intense red fluorescence at the cell nucleus (Fig. 1A). We showed the cell morphology in Differential Interference Contrast (DIC, lower panels of Fig. S2). The chromosomes were also labeled with red fluorescence, as shown in the mitotic body in Fig. S3A. These results confirm the labeling of the cellular nuclei in immortalized DPCs (mSt-DPCs-K4DT). AR with an Azami green monomer was introduced into mSt-DPCs-K4DT using the QCXIP retrovirus vector. Double-transfected cells were selected with 1 μg/mL of puromycin and 1 mg/mL of G418. As shown in Fig. 1B, the mass cell population resistant to puromycin and G418 had a varying expression of green fluorescence and consistently high expression of red fluorescence among the resistant cell population. The variation in the expression of green fluorescence and constant expression of red fluorescence could be explained by the length of the cDNA insert between AR and histone H2B (AR with Azami tag was 3.4 kb and H2B with mStrawberry was 1.2 kb). To avoid expression differences among the cell populations, cell dilution was conducted using 300 cell/10 cm diameter dishes, and cell cloning was repeated with the ring cylinder method at least twice/per cell line. We obtained two independent clones (7 and 10) that highly expressed AR with the Azami green tag and histone H2B with the mStrawberry tag (Fig. 2A and B).

3.2. Detection of the genomic insertion of the expression cassettes and recombinant proteins in DPCs

PCR was conducted to assess the genomic insertion of the expression cassettes of AR with Azami green tag and histone H2B with mStrawberry (Fig. 3A). To ensure the recovery of genomic DNA, the human tuberous sclerosis type 2 gene (TSC2) was amplified (Fig. 3A, right side). As expected, AR with Azami tag and histone H2B with mStrawberry tag were amplified in cloned DPCs-K4DT cells (Fig. 3A, left side). To detect the protein expression of recombinant AR, we performed western blotting using AR-specific antibody (Fig. 3B, left side, Fig. S5). We detected a specific signal of approximately 130 kDa, which is the expected molecular weight of AR with an Azami tag. We also detected a signal at approximately 110 kDa, which indicated stable expression of the AR receptor with the HA tag (Fukuda et al., 2020) (Fig. 3B, panel of anti-AR). We previously established DPC cell lines that stably express AR with an HA protein tag. We also detected the signals around 100 kDa in K4DT AR(HA) and LNcap. FGC. The multiple bands were detected in a lower molecular weight area than the expected size of 130 kDa, which the protein degradation could explain. Since the original AR would be

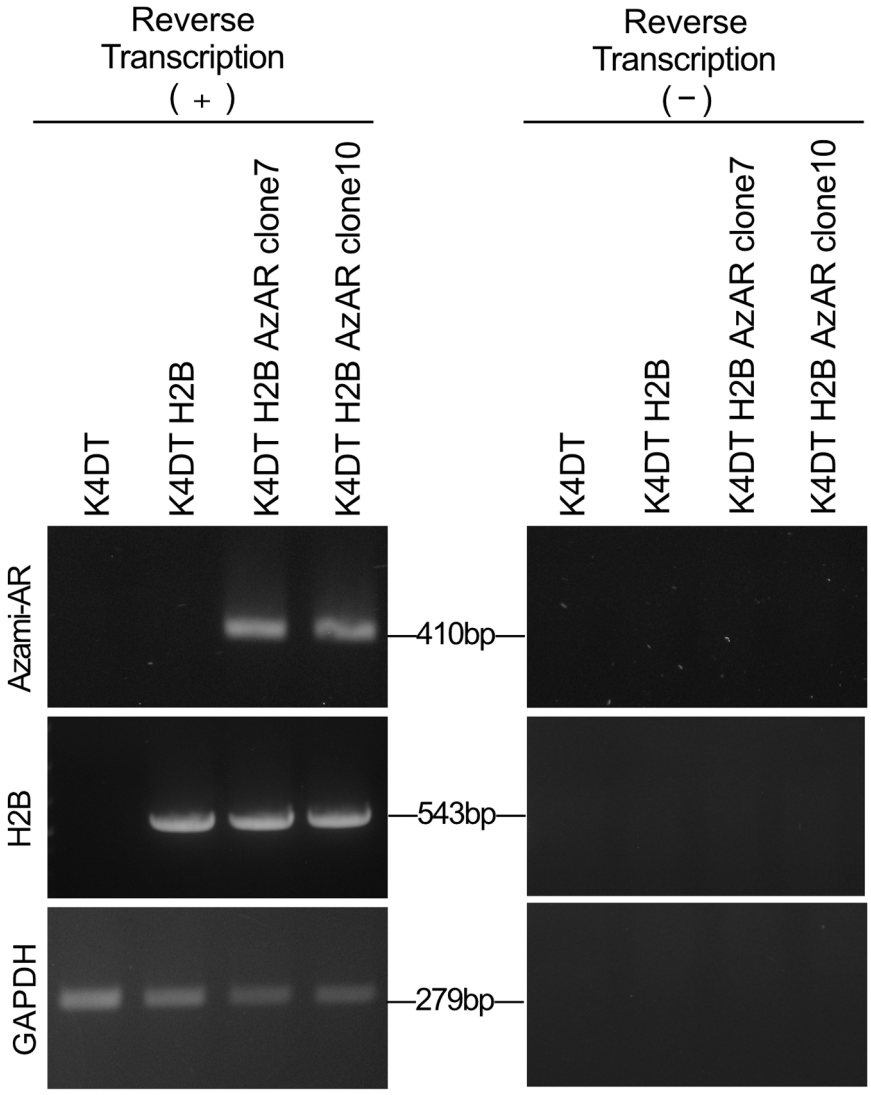

Fig. 4. Detection of expression cassette of Azami green-labeled AR and mStrawberry-labeled H2B at mRNA level using RT-PCR. Left side panels, Detections of Azami AR, H2B expression cassettes at mRNA level. GAPDH is internal control. Right side panels, Detection of Azami Ar, H2B expression cassette under the no existence of reverse transcriptase.

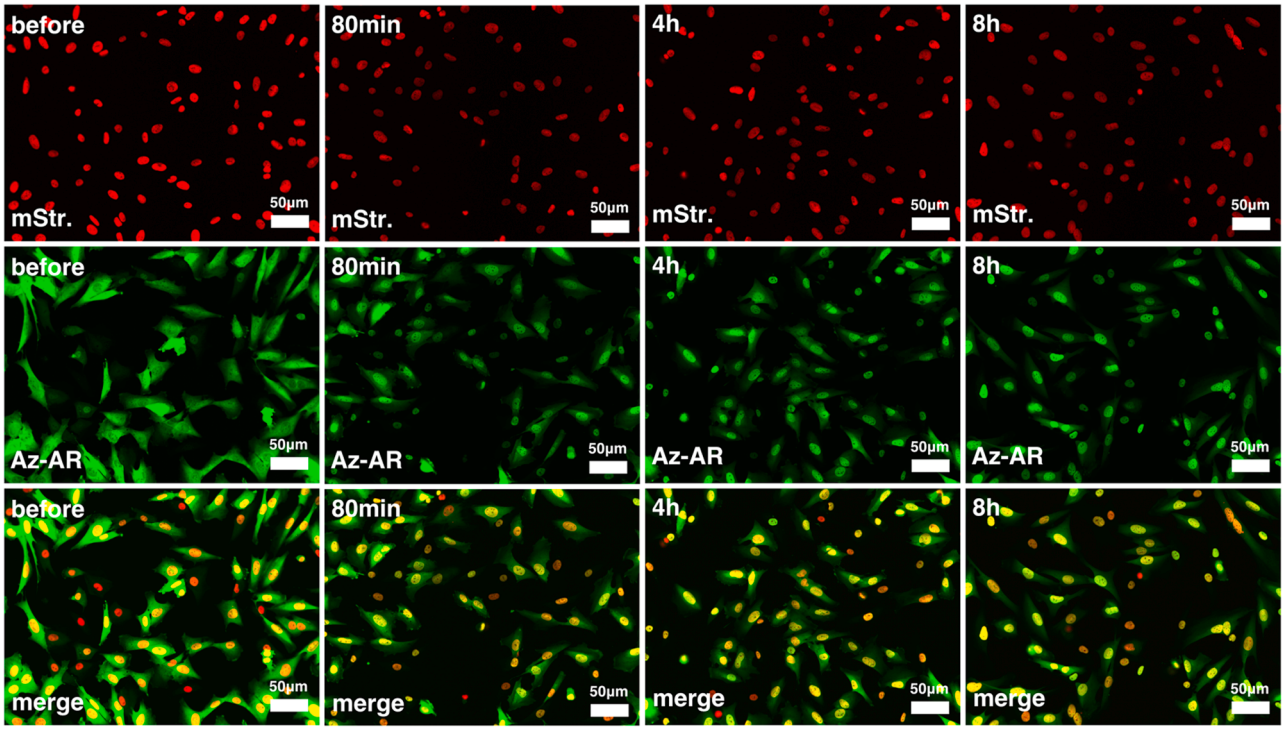

Fig. 5. Detection of the nuclear translocation of Azami green-labeled AR in immortalized DPCs (clone 10) after dihydroxy testosterone (DHT) treatment. The red channel shows the signal of mStrawberry-labeled histone H2B. The green channel shows Azami's green-labeled AR. Images before the exposure of DHT, 80 min after DHT treatment, 4 h after DHT treatment, and 8 h after DHT treatment. After the ligand stimulation, we obtained images from randomly selected area on cell culture dish.

around 110 kDa, fusion with the fluorescence tag could be unstable due to its larger molecular weight. Our detected signal was confirmed to react against the Azami green antibody (Fig. 3B, panel of anti-Azami). We furthermore detected the expression of Strawberry tagged H2B protein at expected molecular weight around 45 kDa (Fig. 3B, panel of anti-Strawberry). α-Tubulin was employed as a loading control for total protein (Fig. 3B and Fig. S5). We obtained two cell lines of immortalized DPCs expressing AR and histone H2B with fluorescence tags. Furthermore, the expression level of established stable AR expressing DPCs is almost identical to the endogenous expression level in LNCap FDG. In addition to the western blots, we performed the RT-PCR to detect Azami AR and strawberry H2B at the mRNA level. In Fig. 4 and S6, we detected the positive signals in RT-PCR of Azami AR and strawberry H2B. The signals were detected with the expected combination of the samples at the expected molecular weight. Furthermore, we did not detect any signals without using reverse transcriptase under the same amplification condition, indicating that our detected signals are derived explicitly from mRNA.

3.3. Time course experiments to detect the nuclear translocation of AR

We conducted time course experiments after ligand stimulation of AR (100 μM DHT). As shown in Fig. 5 (most left panels), AR existed ubiquitously in the nucleus and cytoplasm. Furthermore, the cytoplasm and nucleus were positive in the double transgenic cells. At 80 min after DHT stimulation, the green AR signal accumulated in the nucleus (the cellular organ exhibits red fluorescence, Fig. 5). The cell conditions at 4 and 8 h after DHT stimulation were also analyzed (Fig. 5, middle-right and rightmost panels). From this data, we speculated that the Azami green labeled Androgen receptor shows nuclear translocation starts around 80 minutes after the DHT stimulation.

3.4. Time-lapse imaging analysis to detect the nuclear translocation of AR in DPCs under live cell conditions

Based on these findings, we concluded that time-lapse imaging is essential to obtain the location of AR labeled with a green fluorescence tag and cell nuclei labeled with a red fluorescence tag under live conditions. We used a time-lapse imaging device and maintained cells at 37 °C and 5 % CO_2 with high humidity. In addition to the culture conditions, we used double ND filters (NF10 and NF20) and ProLong™ Live Antifade Reagent (Thermo Fisher Scientific) as an additive to prevent phototoxicity during the microscopic observation. Under these optimized conditions, images were captured through the green and red fluorescence channels and processed into time-lapse and live imaging videos after DHT stimulation (Movie 1, https://doi.org/10.6084/m9.figshare.20456211.v1). As shown in Movie 1, the AR signal (green fluorescence) was detected in both the nucleus and cytoplasm. As the nucleus exhibited red fluorescence, the color of the cell nucleus became orange. Approximately 20 min after DHT stimulation (image was obtained every 1 min), the color of the cell nucleus became lemon-yellow due to the accumulation of fluorescence-labeled AR, indicating that the color of the nucleus is due to the nuclear translocation of AR from the cytoplasm of DPCs.

Supplementary material related to this article can be found online at doi:10.1016/j.tice.2024.102631.

3.5. Quantitative Detection of cytoplasmic and nuclei signal intensities using image analysis

We proceeded to detect the nuclear accumulation of AR using image processing quantitatively. The position of the cellular nucleus was detected using the red fluorescence channel. Image analysis of the red channel revealed that the shape of the cellular nucleus was detected as a masked area after binarization. The threshold of binarization was optimized to detect the most appropriate area that could be selected from

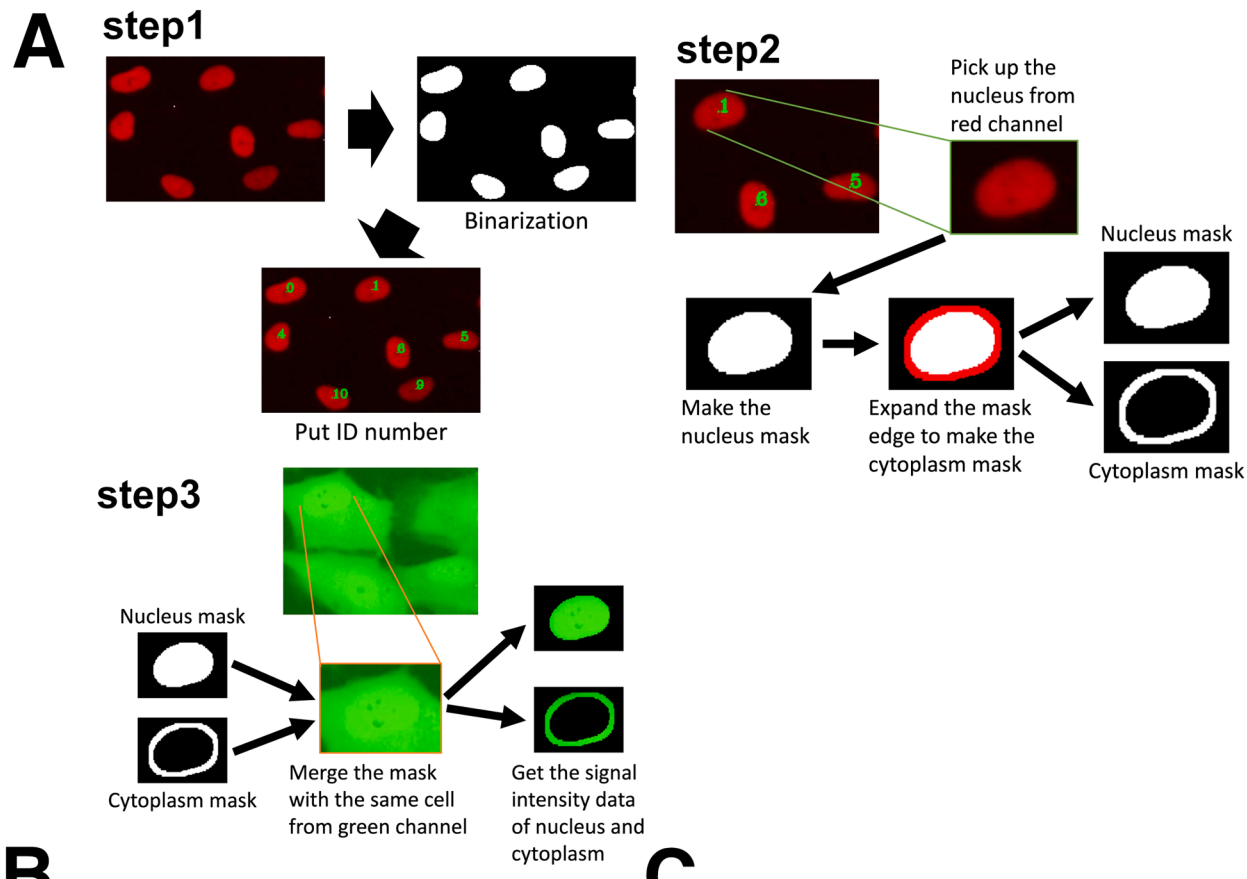

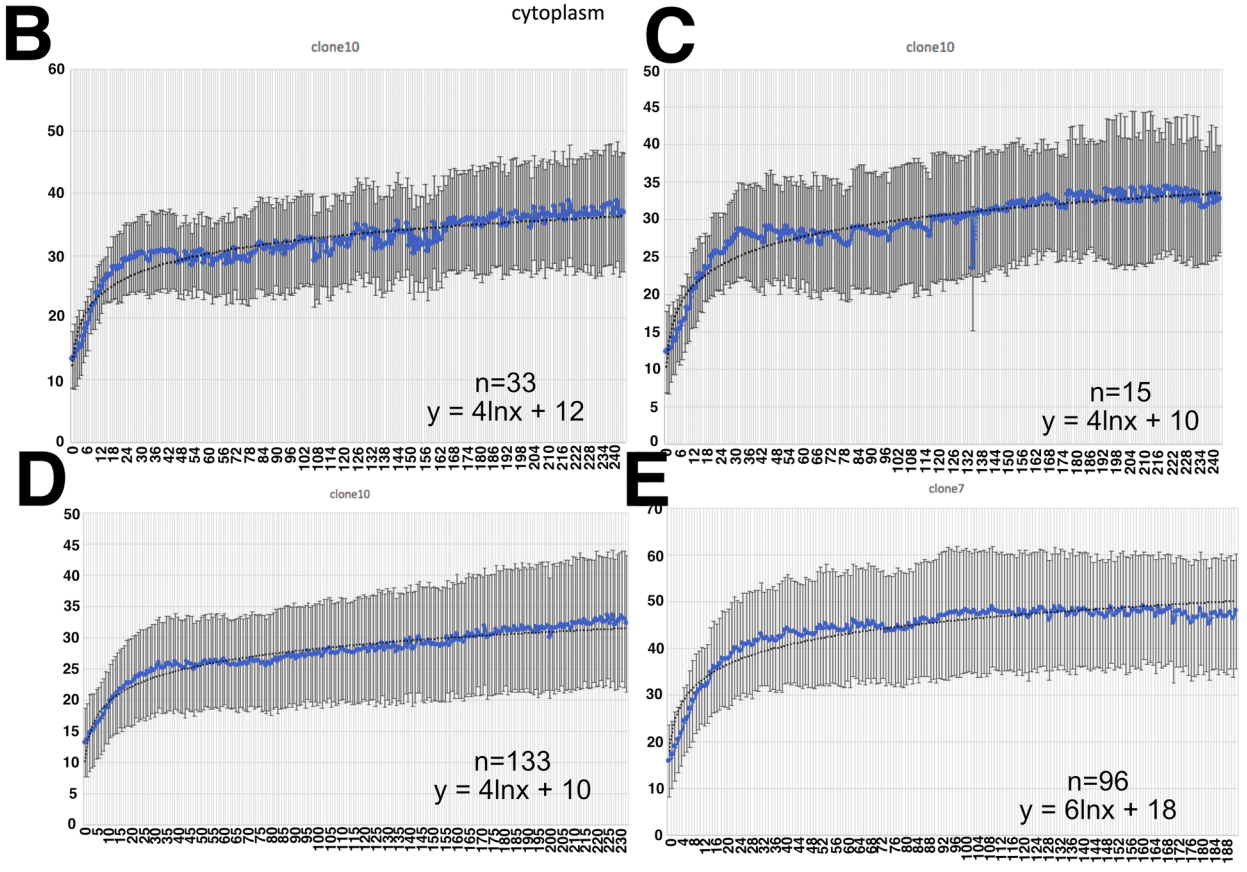

(caption on next page)

Fig. 6. The strategy for measuring fluorescence intensity in the nucleus and cytoplasm of immortalized DPCs using the digital mask technique from the time-lapse live imaging video. A Process of the digital image analysis of cells. The shape information of nuclei was extracted from the binarized image of the red channel, nuclear mask (step 1). From the nuclear mask, we expanded the mask edge to obtain the location information of the cytoplasm (step 2). Based on the mask shape information of the nuclei and cytoplasm obtained from the red channel, we measured the signal intensity of the green channel (not the red channel) within the nuclei mask and cytoplasm mask (step 3). Please see the independent manuscript (Fukasawa M., et al., 2024, see reference (Fukasawa et al., 2024)) for the detailed information. B, The average value of the nuclear/cytoplasm fluorescence intensity (blue line) and standard deviation (SD) in clone 10. Images of 33 cells were analyzed. The approximate formula (black line): $y = 4\ln x + 12$. The y-axis indicates the Nuclear/cytoplasm ratio of fluorescence intensity, and the X-axis indicates the frame number. Image capture was performed every 40 seconds in each frame. Therefore, frame 30 is the 20-minute time point after the start of DHT. C, The average nuclear/cytoplasm fluorescence intensity (blue line) and standard deviation (SD) in clone 10. Images of 15 cells were analyzed. The approximate formula (black line): $y = 4\ln x + 10$. D, The average value of nuclear/cytoplasm fluorescence intensity (blue line) and standard deviation (SD) in clone 10, combined from four independent videos. Images of 133 cells were analyzed. The approximate formula (black line): $y = 4\ln x + 10$. E, The average value of nuclear/cytoplasm fluorescence intensity (blue line) and standard deviation (SD) in clone 7 based, obtained from four independent videos. The total cell number is 96. The approximate formula (black line): $y = 6\ln x + 18$.

the cellular morphology of cell images in the red channel (see Fig. 6A and section on Signal quantitation of nuclei and cytoplasm in materials and method). The fluorescence intensity through the green channel within the masked area of the nuclei was detected via image quantitation after monochrome data conversion. The shape information of the nuclei was extracted from the binarized image of the red channel (i.e., nuclear mask, step 1). Based on the nuclear mask, we expanded the mask edge to obtain the location information of the cytoplasm (step 2). Using the mask shape information of the nuclei and cytoplasm from the red channel, we measured the signal intensity of the green channel (not the red channel) within the nuclei mask and cytoplasm mask (step 3). Based on our developed algorithm, quantitative information can be obtained in an automatic manner using computer programming. Detailed algorism to detect the nuclei and cytoplasm has been published as an independent manuscript (Fukasawa et al., 2024). Briefly, we measured each cell with a unique ID number and the change in the signal intensity of each cell using a time course analysis. The video with the unique cell ID is listed as Movie 2 (merged images of green and red fluorescence channels, https://doi.org/10.6084/m9.figshare.20456376.v2). As observed in the video, when the nuclei are too close or overlap, the program cannot recognize cell localization, and cell labeling disappears. Currently, we are attempting to solve the close and overlap issues using a modified algorithm (Fukasawa et al., 2024). The time-lapse video of the green fluorescence channel is shown in Movie 3 (https://doi.org/10.6084/m9.figshare.20456472.v3) and that of the red fluorescence channel is shown in Movie 4 (https://doi.org/10.6084/m9.figshare.20456406.v2). Graphs of the nuclei/cytoplasm ratios obtained from the three independent movies of clone 10 were plotted (Fig. 6B, C). We combined the results of four movies of clone 10 in total 133 cells as Fig. 6D The following formula was obtained from the clone 10 data: $y = 4\ln x + 10$ (Fig. 6D). Furthermore, we also showed the four movies of clone 7 in total 96 cells as Fig. 6E. The raw data of Fig. 6D is presented in Figshare (Table 1, https://doi.org/10.6084/m9.figshare.18095756). The nuclei/cytoplasm ratio plateaued approximately 20 min after exposure to DHT.

Supplementary material related to this article can be found online at

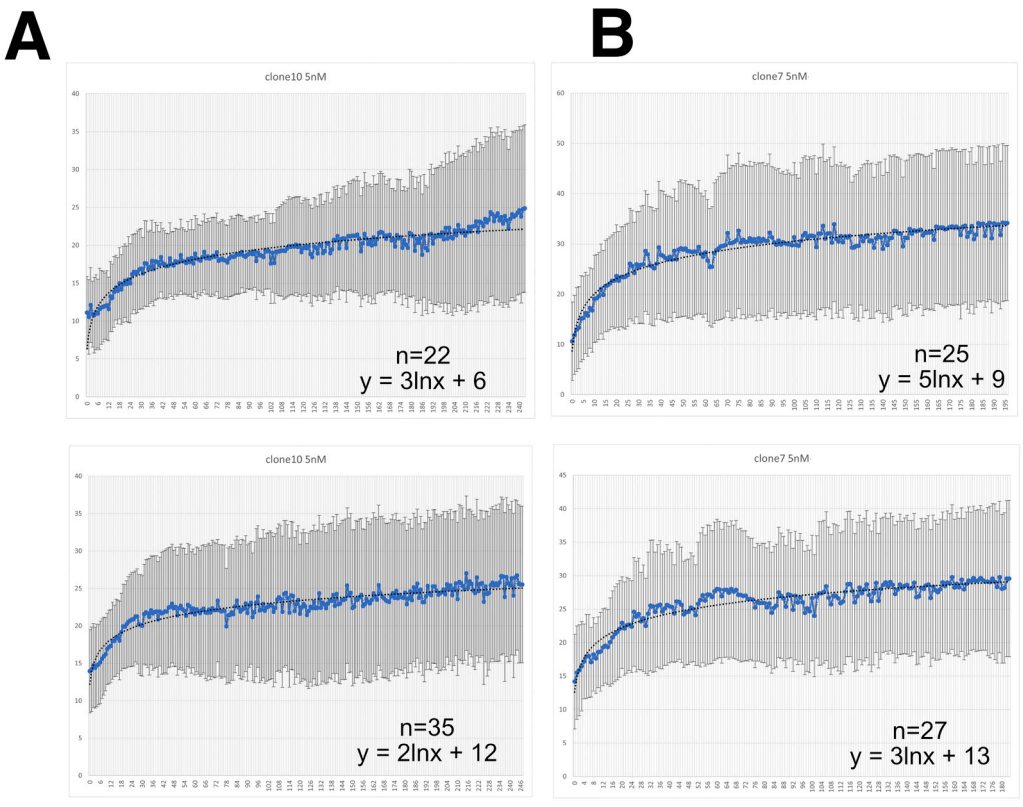

Fig. 7. The average value of the nuclear/cytoplasm fluorescence intensity (blue line) and standard deviation (SD) in clones 10 and 7 treated with 5 nM DHT. The Y-axis indicates the Nuclear/cytoplasm ratio of fluorescence intensity, and the X-axis indicates the frame number. A, Nuclear/cytoplasm fluorescence intensity in clone 10. The results of two independent videos (upper and lower panels) were shown. B, Nuclear/cytoplasm fluorescence intensity in clone 7. The results of two independent videos (upper and lower panels) were shown. The standard deviation is more significant than that obtained with 100 nM DHT (Fig. 5).

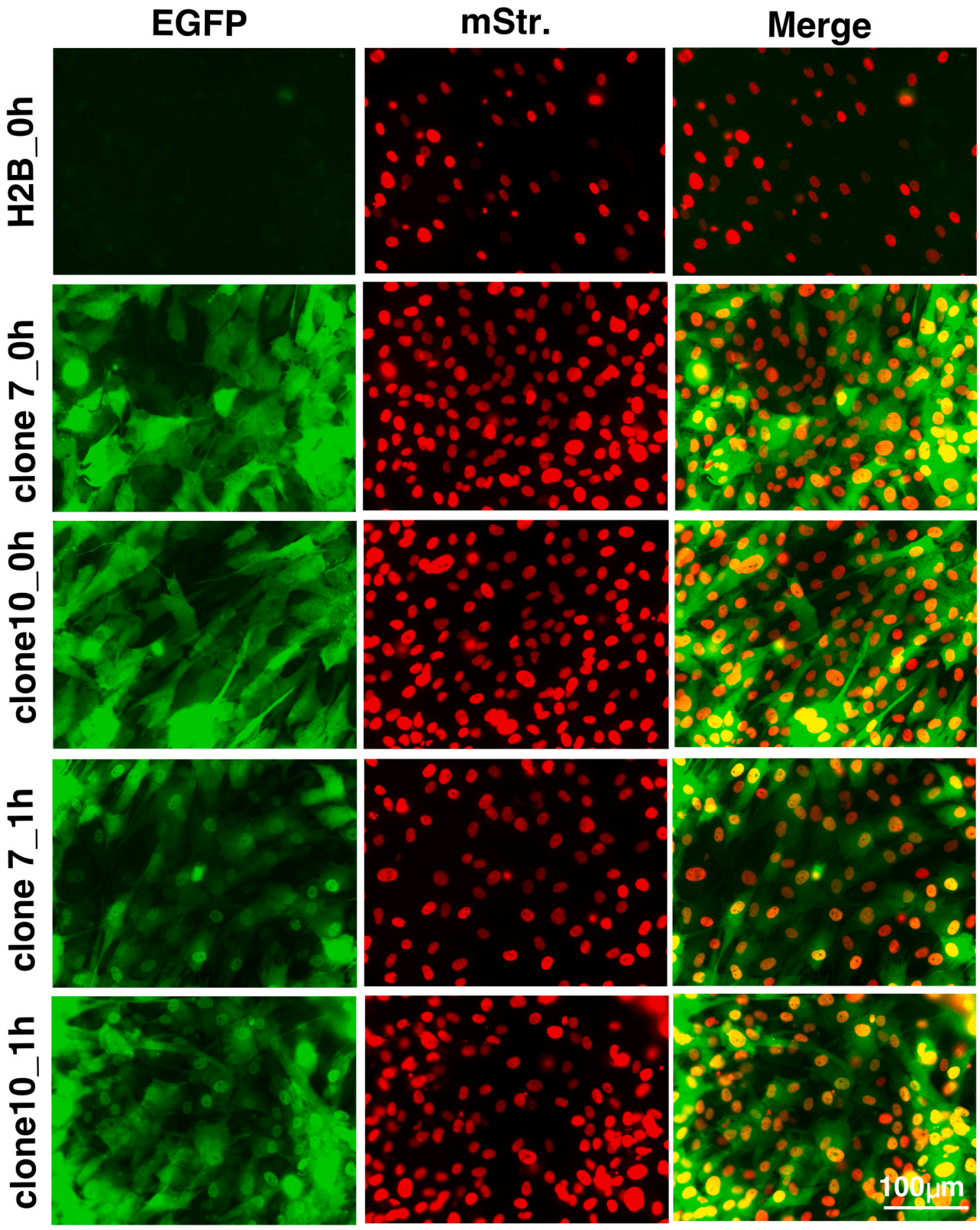

Fig. 8. Detection of nuclear translocation of Androgen receptor with Azami green fluorescence tang after the testosterone treatment of 100 nM. H2B_0h indicates the cell images obtained from DPCs which only expresses mStrawberry-labeled H2B just after the ligand stimulation. No green fluorescence. Clone 7_0h indicates the cell images obtained from the DPC of clone 7, which expresses mStrawberry-labeled H2B and Azami green-tagged AR just after the ligand stimulation. Clone 10_0h indicates the cell images obtained from the DPC of clone 10, which expresses mStrawberry-labeled H2B and Azami green-tagged AR just after the ligand stimulation. Clone 7_1h indicates the cell images obtained from DPC of clone 7, which expresses mStrawberry-labeled H2B, and Azami green-tagged AR at 1 hour after the ligand stimulation. Clone 10_1h indicates the cell images obtained from DPC of clone 10, which expresses mStrawberry-labeled H2B and Azami green-tagged AR at 1 hour after the ligand stimulation.

doi:10.1016/j.tice.2024.102631.

Finally, the nuclear/ cytoplasm ratio was obtained under exposure to 5 nM DHT. Fig. 7A and B show that data were obtained from clones 10 and 7. The graphs show that the nuclear/ cytoplasm ratio plateaued at approximately 20 min, suggesting that treatment with 5 nM DHT induces nuclear translocation at almost the same speed as 100 nM DHT. However, the standard deviation of the signal ratio for 5 nM is larger than that for 100 nM. The larger standard deviation is because 5 nM would not be a sufficient dose to obtain reproducible data.

We also detected whether other types of ligand stimulation, such as testosterone, introduce nuclear translocation. As shown in Fig. 8, clone 7 and clone 10 showed translocation into the nuclei. The nuclear translocation was detected around 30 minutes after the testosterone treatment. From this data, we concluded that testosterone and DHT also work as ligand stimulation.

4. Discussion

In this study, we established immortalized DPCs with constant AR and histone H2B expression with the Azami green and mStrawberry fluorescence tags, respectively. Stable double transformants were established via retroviral gene transfer. Previously, we revealed that our established immortalized DPCs maintained the original condition of human chromosomes (Fukuda et al., 2020). The immortalized cells are associated with easy handling as research materials.

In DPCs, testosterone signaling is a critical factor in the progression of AGA. The affinity of DHT for AR is stronger than that of testosterone. To inhibit AR signaling, the inhibition of 5 alpha-reductase is the first clinical option against AGA. Although the inhibition of 5 alpha-reductase results in a lower amount of DHT, the production of testosterone itself is not affected by 5 alpha-reductase. Receptor translocation is an essential step in detecting AR signaling.

We proposed a method for monitoring the translocation of the AR from the cytoplasm to the nucleus. Translocation to the nucleus is the key limiting step in steroid hormone signaling. The nuclear translocation of AR can be quantified under stable conditions. Furthermore, the nuclear/cytoplasm ratio was detected via imaging analysis.

The image analysis algorithm in this study allowed us to monitor the cell condition efficiently. Several image acquisition, processing and signal quantification software are available from imaging equipment manufacturers (Kumar et al., 2021). Imaging software allows us to measure the signal ratio of the nuclear and cytoplasm efficiently; even more than 200 cells exist in the frame. However, there is one point that our study has a technical novelty. In the previous method, the quantitation of signal within the nuclei required the process of human work in every frame of the images since previous software simply output the nuclear and cytoplasm signal. We need to address which cell corresponds to which cell at an earlier frame by human efforts since cell location changes every frame, and the speed and direction of movement are not constant. That process requires tremendous human efforts, and measuring the signal intensity of more than 100 cells in 200 images is impractical. Our system allows quantitative Detection of the nuclear translocation of AR automatically using computer programming. Our developed algorithm enabled the Detection of the nuclear shape and measurement of the signal's nuclear/ cytoplasm ratio. However, the number of cells recognized by the program is limited when the distance between cell to cell is too close. Currently, we are trying to resolve this problem to improve the labeling ratio. Furthermore, we plan to develop the stand-alone computer application software by collaborating with a software company. Our method might allow us to screen candidate inhibitors of the nuclear translocation of AR. These chemicals could be helpful in inhibiting testosterone signaling, which would be beneficial against prostate cancer.

5. Conclusion

In this study, we established the immortalized DPC expressing androgen receptor and histone H2A, which were labeled with two fluorescence colors. Nuclear receptor transition was detected with time lapse imaging, and the intensities of cytoplasm and nuclear was quantitatively detected. Since this cell is immortalized and easiness of the handling, established cell lines would be beneficial as the research material.

CRediT authorship contribution statement

Eriko Sugano: Supervision, Project administration, Conceptualization. **Taku Ozaki:** Supervision, Project administration, Conceptualization. **Haruka Tate:** Data curation. **Sayo Kashiwagi:** Project administration, Methodology, Conceptualization. **Mizuki Fukasawa:** Software, Resources, Methodology, Formal analysis, Data curation. **Tao Wu:** Methodology, Data curation, Conceptualization. **Lanlan Bai:** Methodology, Investigation, Formal analysis, Data curation, Conceptualization. **Tomokazu Fukuda:** Writing – review & editing, Writing – original draft, Visualization, Validation, Supervision, Software, Resources, Project administration, Methodology, Investigation, Funding acquisition, Formal analysis, Data curation, Conceptualization. **Takuya Akashi:** Resources, Conceptualization. **Tsuyoshi Ishii:** Supervision, Resources, Conceptualization. **Hiroshi Tomita:** Supervision, Conceptualization. TF, TW, MF, LB, KF, HT, TA performed the experiments and obtained the data. SK, TO, ES, HT, TI, TF, TA contributed to the experimental design of the study. TF, TW, MF, TA wrote the paper. All authors reviewed the manuscript. We appreciate the mentorship provided by Dr. Tohru Kiyono (Exploratory Oncology Research and Clinical Trial Center, National Cancer Center) for the cell culture work and cell immortalization..

Acknowledgement

We thank Takahashi Kouhei, M.Sc. and Shin Takase, B.Sc. for conducting the pilot study to establish the immortalized DPCs.

Appendix A. Supporting information

Supplementary data associated with this article can be found in the online version at doi:10.1016/j.tice.2024.102631.

Data availability

Data will be made available on request.

References

Chiu, C.L., Patsch, K., Cutrale, F., Soundararajan, A., Agus, D.B., Fraser, S.E., Ruderman, D., 2016. Intracellular kinetics of the androgen receptor shown by multimodal Image Correlation Spectroscopy (mICS). Sci. Rep. 6, 22435.

Choi, G.S., Kim, J.H., Oh, S.Y., Park, J.M., Hong, J.S., Lee, Y.S., Lee, W.S., 2016. Safety and tolerability of the dual 5-alpha reductase inhibitor dutasteride in the treatment of androgenetic alopecia. Ann. Dermatol. 28, 444–450.

Deppert, W., 2007. Mutant p53: From guardian to fallen angel? Oncogene 26.

Donai, K., Kuroda, K., Guo, Y., So, K.-H., Sone, H., Kobayashi, M., Nishimori, K., Fukuda, T., 2013. Establishment of a reporter system to monitor silencing status in induced pluripotent stem cell lines. Anal. Biochem. 443, 104–112.

Fizazi, K., Massard, C., Bono, P., Jones, R., Kataja, V., James, N., Garcia, J.A., Protheroe, A., Tammela, T.L., Elliott, T., Mattila, L., Aspegren, J., Vuorela, A., Langmuir, P., Mustonen, M., 2014. Activity and safety of ODM-201 in patients with progressive metastatic castration-resistant prostate cancer (ARADES): an open-label phase 1 dose-escalation and randomised phase 2 dose expansion trial. Lancet Oncol. 15, 975–985.

Fukasawa, M., Fukuda, T., Takuya Akashi, N., 2024. Method of tracking and analysis of fluorescent-labeled cells using automatic thresholding and labeling. IEEJ Trans. xx 1–5.

Fukuda, T., Furuya, K., Takahashi, K., Orimoto, A., Sugano, E., Tomita, H., Kashiwagi, S., Kiyono, T., Ishii, T., 2021. Combinatorial expression of cell cycle regulators is more

suitable for immortalization than oncogenic methods in dermal papilla cells. iScience 24, 101929.
Fukuda, T., Mishina, Y., Walker, M.P., DiAugustine, R.P., 2005. Conditional transgenic system for mouse aurora A kinase: degradation by the ubiquitin proteasome pathway controls the level of the transgenic protein. Mol. Cell. Biol. 25, 5270–5281.
Fukuda, T., Takahashi, K., Takase, S., Orimoto, A., Eitsuka, T., Nakagawa, K., Kiyono, T., 2020. Human derived immortalized dermal papilla cells with a constant expression of testosterone receptor. Front. Cell Dev. Biol. 8, 157.
Fukuda, T., Tani, Y., Kobayashi, T., Hirayama, Y., Hino, O., 2000. A New Western Blotting Method Using Polymer Immunocomplexes: detection of Tsc1 and Tsc2 Expression in Various Cultured Cell Lines. Anal. Biochem. 285, 274–276.
Georget, V., Lobaccaro, J.M., Terouanne, B., Mangeat, P., Nicolas, J.C., Sultan, C., 1997. Trafficking of the androgen receptor in living cells with fused green fluorescent protein-androgen receptor. Mol. Cell. Endocrinol. 129, 17–26.
Kumar, S., Kashyap, J., Thakur, K., Tyagi, R.K., 2021. A simple method for visual assessment and quantification of altered subcellular localization of nuclear receptors. Nucl. Recept. Art. Sci. Modul. Des. Discov. 23–36.
Kwack, M.H., Sung, Y.K., Chung, E.J., Im, S.U., Ahn, J.S., Kim, M.K., Kim, J.C., 2008. Dihydrotestosterone-Inducible Dickkopf 1 from balding dermal papilla cells causes apoptosis in follicular keratinocytes. J. Invest. Dermatol. 128, 262–269.
Marcelli, M., Stenoien, D.L., Szafran, A.T., Simeoni, S., Agoulnik, I.U., Weigel, N.L., Moran, T., Mikic, I., Price, J.H., Mancini, M.A., 2006. Quantifying effects of ligands on androgen receptor nuclear translocation, intranuclear dynamics, and solubility. J. Cell. Biochem. 98, 770–788.
Nadal, M., Prekovic, S., Gallastegui, N., Helsen, C., Abella, M., Zielinska, K., Gay, M., Vilaseca, M., Taulès, M., Houtsmuller, A.B., Van Royen, M.E., Claessens, F., Fuentes-Prior, P., Estébanez-Perpiñá, E., 2017. Structure of the homodimeric androgen receptor ligand-binding domain. Nat. Commun. 8, 14388.
Said, M.A., Mehta, A., 2018. The impact of 5α-reductase inhibitor use for male pattern hair loss on men's health. Curr. Urol. Rep. 19.
Saitoh, M., Takayanagi, R., Goto, K., Fukamizu, A., Tomura, A., Yanase, T., Nawata, H., 2002. The presence of both the amino- and carboxyl-terminal domains in the ar is essential for the completion of a transcriptionally active form with coactivators and intranuclear compartmentalization common to the steroid hormone receptors: a three-dimensional imaging study. Mol. Endocrinol. 16, 694–706.
Szafran, A.T., Szwarc, M., Marcelli, M., Mancini, M.A., 2008. Androgen receptor functional analyses by high throughput imaging: determination of ligand, cell cycle, and mutation-specific effects. PLoS One 3, e3605.
Tomura, A., Goto, K., Morinaga, H., Nomura, M., Okabe, T., Yanase, T., Takayanagi, R., Nawata, H., 2001. The subnuclear three-dimensional image analysis of androgen receptor fused to green fluorescence protein. J. Biol. Chem. 276, 28395–28401.
Tyagi, R.K., Lavrovsky, Y., Ahn, S.C., Song, C.S., Chatterjee, B., Roy, A.K., 2000. Dynamics of intracellular movement and nucleocytoplasmic recycling of the ligand-activated androgen receptor in living cells. Mol. Endocrinol. 14, 1162–1174.
York, K., Meah, N., Bhoyrul, B., Sinclair, R., 2020. A review of the treatment of male pattern hair loss. Expert Opin. Pharmacother. 21, 603–612.
Zacharias, D.A., Violin, J.D., Newton, A.C., Tsien, R.Y., 2002. Partitioning of lipid-modified monomeric GFPs into membrane microdomains of live cells. Science 296, 913–916.